Supporting Information

Biomass-derived cobalt/ carbon hierarchically structured composites for efficient oxygen electrocatalysis and zinc–air batteries

Jing Chen,[ab] *Shaoxuan Yang,**[ab] *Zhengping Zhang**[ab] *and Feng Wang**[ab]

[a] State Key Laboratory of Chemical Resource Engineering, Beijing Key Laboratory of Electrochemical Process and Technology for Materials, Beijing University of Chemical Technology, Beijing 100029, P R China
[b] Beijing Advanced Innovation Center for Soft Matter Science and Engineering, Beijing University of Chemical Technology, Beijing 100029, P. R. China

*E-mail: wangf@mail.buct.edu.cn
*E-mail: zhangzhengping@mail.buct.edu.cn
*E-mail: ysx@mail.buct.edu.cn

1. Experimental Section

Chemicals. bovine serum albumin, [BSA, separating from the fresh blood], sodium hydroxide [NaOH, Sinopharm, CAS#: 1310-73-2], cobalt chloride hexahydrate [$CoCl_2 \cdot 6H_2O$, Sinopharm, CAS#: 7791-13-1], ethanol, [C_2H_6O, Sinopharm, CAS#: 64-17-5], potassium hydroxide [KOH, Aladdin, CAS#: 1310-58-3], Nafion [5%, DuPont], and 20% Pt/C [Alfa Aesar] were used without further purification. High purity oxygen and nitrogen gas were bought from Beijing AP BAIF Gases Industry Co. Ltd.

Preparation of Co@Co-N,S-C. Cobalt chloride (10 g) and BSA powders (2 g) were dispersed in deionized water (70 mL), respectively. The BSA dispersion was stirred at 60 ℃ for 30 minutes, then 6 mL NaOH solution (0.5 M) and the cobalt chloride solution were added dropwise. The resulting slurry was stirred at 60 ℃ for half an hour, then dried and ground into powders. A proper amount of above precursor was placed into a quartz boat, heated to 800 °C in Ar atmosphere for 2 hours (heating rate was 5 ℃ min^{-1}). After cooling to room temperature, the product was leached with dilute hydrochloric acid, and a secondary heat treatment was performed under the same conditions for 1 hour. After cooling to room temperature, Co@Co-N,S-C was obtained.

Preparation of Co-N,S-C. Co-N,S-C was prepared following the similar procedures as Co@Co-N,S-C. Notably, the pyrolyzed products before acid leaching was ball milled (400rpm for 2 hours) to remove Co nanoparticles encapsulated in graphitic carbon.

Preparation of N,S-C. N,S-C was prepared by direct pyrolysis of BSA powders at 800 °C in Ar atmosphere for 2 hours (heating rate was 5 ℃ min^{-1}).

Materials characterizations

Field-emission scanning electron microscopy (FE-SEM, JSM-6701/JEOL) and high-resolution transmission electron microscopy (HR-TEM, Tecnai G2 F30/FEI) were used to observe the morphologic and structural characteristics of the samples. Fourier transform infrared spectroscopy from 4000 to 500 cm^{-1} was carried out on a Nicolet 8700/Continuum XL (Thermo Scientific). Raman spectra were record on a Horiba Jobin Yvon LabRam HR800 with an excitation wavelength of 633 nm. The X-ray diffraction profile (XRD) was obtained on a Rigaku D/Max 2500 VB2+/PC diffractometer with Cu Ka radiation (λ=1.54056 Å) as the X-ray source. Chemical compositions and elemental oxidation states of the samples were investigated by X-ray photoelectron spectrum (XPS, Thermo Fisher Scientific ESCALAB 250). The surface area was measured by nitrogen adsorption-desorption isotherms using the Brunauer-Emmett-Teller (BET) method on Micromeritics ASAP 2460. Thermogravimetric analysis was performed on a STA7300 (HITACHI) in an argon atmosphere. The temperature was programmed to rise with heating rate of 10 °C min^{-1} from 30 to 900 °C. Elemental analyzer was performed on an Elementar vario El cube.

The Co *K*-edge XAFS spectra were acquired at beamline 1W1B station of the Beijing Synchrotron Radiation Facility, China. The Co K-edge XANES data were recorded in a fluorescence mode using a Lytle detector. Co foil, Co_3O_4, Co phthalocyanine were used as references. The storage ring was working at the energy of 2.5 GeV with a maximum current of 250 mA. The acquired EXAFS data was processed according to the standard procedures using the ATHENA module implemented in the IFEFFIT software packages.[1,2] The k^3-weighted EXAFS spectra were obtained by subtracting the post-edge background from the overall absorption and then normalizing with respect to the edge-jump step. Subsequently, χ(k) data of Co *K*-edge in the k-space ranging from 3.0 to 12.3 $Å^{-1}$ were Fourier transformed to real (*R*)

space using a hanning windows (dk = 1.0 $Å^{-1}$) to separate the EXAFS contributions from different coordination shells.

Electrochemical measurements

The electrochemical tests were carried out in a three-electrode system on a Rotating Ring Disk Electrode Apparatus (RRDE-3A), ALS (BAS INC, Tokyo, Japan). The potential was recorded using potassium chloride (KCl) saturated calomel as the reference electrode. All the potentials were calibrated to the reversible hydrogen electrode (RHE) according to Nernst equation. The loading mass of the as-prepared electrocatalysts on the working electrode was 0.4 mg cm^{-2}. For comparison, commercial 20% Pt/C catalyst obtained from Alfa Aesar was measured. The loading mass of 20% Pt/C samples on the working electrode was 0.2 mg cm^{-2}. All the electrochemical measurements in this work were corrected by the IR compensation (90 %) fuction of CHI 760E.

Rotating disk electrode (RDE) measurements: The glassy carbon rotating disk electrode is 4.0 mm in diameter. The Koutecky–Levich (K-L) plots reflecting the relation of current density (J^{-1}) versus rotation rate ($\omega^{-1/2}$) were constructed according to:

$$J^{-1} = J_k^{-1} + (0.2nFC_{O_2}D_{O_2}^{2/3}\gamma^{-1/6})^{-1}\omega^{-1/2}$$

where J is the measured current, J_k is the kinetic-limiting current, n is the number of electrons transferred per oxygen molecule, F is the Faraday constant (96,485 C mol^{-1}), C_{O_2} is the concentration of oxygen in 0.1 M KOH, D_{O_2} is the diffusion coefficient of oxygen in 0.1 M KOH, γ is the kinematic viscosity of the 0.1 M KOH and ω is the electrode rotation rate.

For the Tafel plot, the kinetic current was calculated from the mass-transport correction of RDE by:

$$J_k = \frac{J \times J_d}{J_d - J}$$

where J_d is the diffusion limited current density.

Rotating ring-disk electrode (RRDE) measurements: The disk electrode was scanned catholically at a rate of 5 $mV \cdot s^{-1}$ and the ring potential was constant at 1.5 V *vs.* RHE. The percentage of hydrogen peroxide yield (*% HO_2^-*) and the corresponding electron transfer number (*n*) was calculated by the followed equation:

$$\% HO_2^- = 200 \times \frac{I_r/N}{I_d + I_r/N}$$

$$n = 4 \times \frac{I_d}{I_d + I_r/N}$$

where I_d is disk current, I_r is ring current and $N = 0.4$ is the current collection efficiency of the Pt ring.

Electrochemical measurements for rechargeable zinc-air batteries.

A measurements of rechargable aqueous zinc-air batteries were performed on home-built electrochemical cells The air electrodes were prepared by uniformly coating the as-prepared catalysts ink on a hydrophobic carbon paper (TGP-H-060, Toray) by ultrasonic sprayer (SP201, Kunshan Sunlaite New Energy Co., Ltd). The ink content of Co@Co-N,S-C coated onto carbon paper was 1.5 mg cm^{-2}. As the reference, an air electrode fabricated by 20% Pt/C and RuO_2 catalysts was prepared as the same procedure, the ink content of 20% Pt/C and RuO_2 was 2 mg cm^{-2}. When constructed a rechargeable Zn-air battery, the above carbon paper coated with catalysts was used as an air cathode, zinc foil was used as the anode, Celgard 2340 microporous membrane as the separator, and 6 M KOH with 0.2 M zinc acetate as electrolyte. All Zn-air

batteries were assembled and tested under ambient conditions. The polarization curves were recorded by linear sweep voltammetry (5 mV s^{-1}, at room temperature) on a CHI760E electrochemical workstation.

Flexible solid-state zinc-air batteries were fabricated with carbon cloth (CeTech W1S1009) supported Co@Co-N,S-C catalysts as cathode, a polished zinc foil as anode, gel polymer as solid electrolyte, and nickel foam as current collector. The solid electrolyte was prepared as follow: polyvinyl alcohol (PVA) powder was added into 10 mL H_2O at 90 ℃ under stirring. After the solution transfer into transparent gel, 1 mL 18 M KOH with 0.02 M zinc acetate was added into the mixture. After being stirred for 0.5 h, the gel was poured onto a glass plate and freezed in a freezer at -20 ℃ for 3 h. The procedure was obtained after thawing at room temperature.

2. Fig.s and Tables.

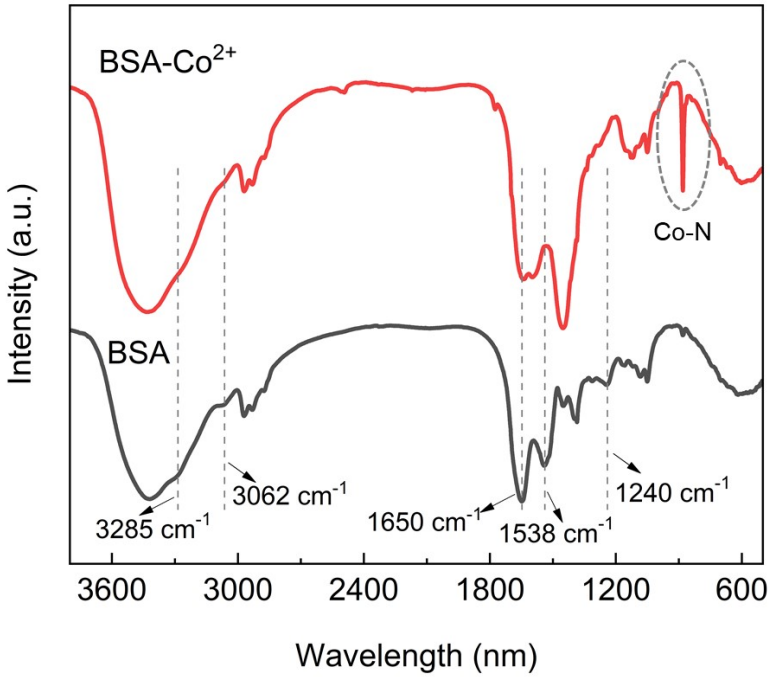

Fig. S1 FTIR spectra of BSA and BSA-Co^{2+}.

The spectrum of BSA showed the characteristic bands of amide A (3285 cm^{-1}), amide B (3062 cm^{-1}), amide I, II, and III (respectively 1650, 1538 and 1240 cm^{-1}).[3,4] After the addition of NaOH and Co^{2+}, the BSA hydrolyzed along with all the characteristic bands reduced; meanwhile, the shifting of amide I and amide II from 1650 and 1538 cm^{-1} to 1639 and 1598 cm^{-1} supported the evidence of Co^{2+} ions interaction with the C=O and N-H groups of BSA. Besides, the spectrum of BSA-Co^{2+} showed the characteristic bands of Co-N (880 cm^{-1}).

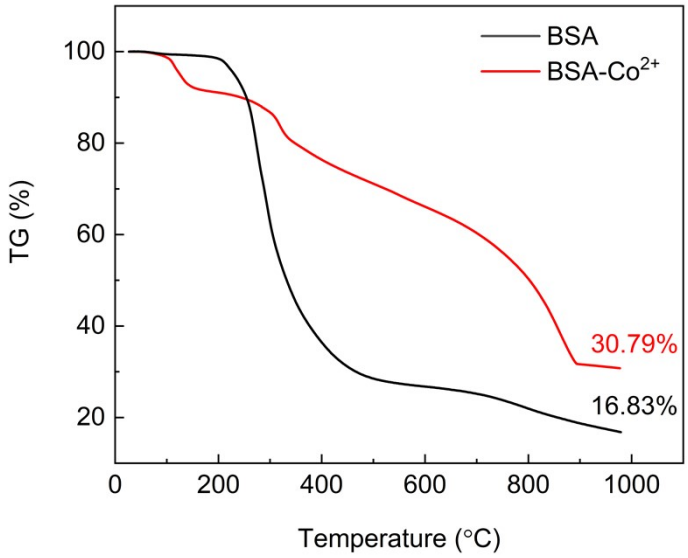

Fig. S2 The TG curves of BSA and BSA-Co^{2+} under Ar atmosphere.

The BSA and BSA-Co^{2+} first occurred the release of physically adsorbed water under 100 ℃. The BSA-Co^{2+} then showed obvious weight loss (105.8−168.7 ℃) attributed to the release of crystal water. The decomposition of proteins was then occurred at 195.2 ℃ for BSA and 237.3 ℃ for BSA-Co^{2+}. The starting shoulders were due to the polypeptide chain thermal decomposition of proteins. The obvious difference in the weight loss process indicated that there was a strong interaction between Co^{2+} ions and protein molecules.

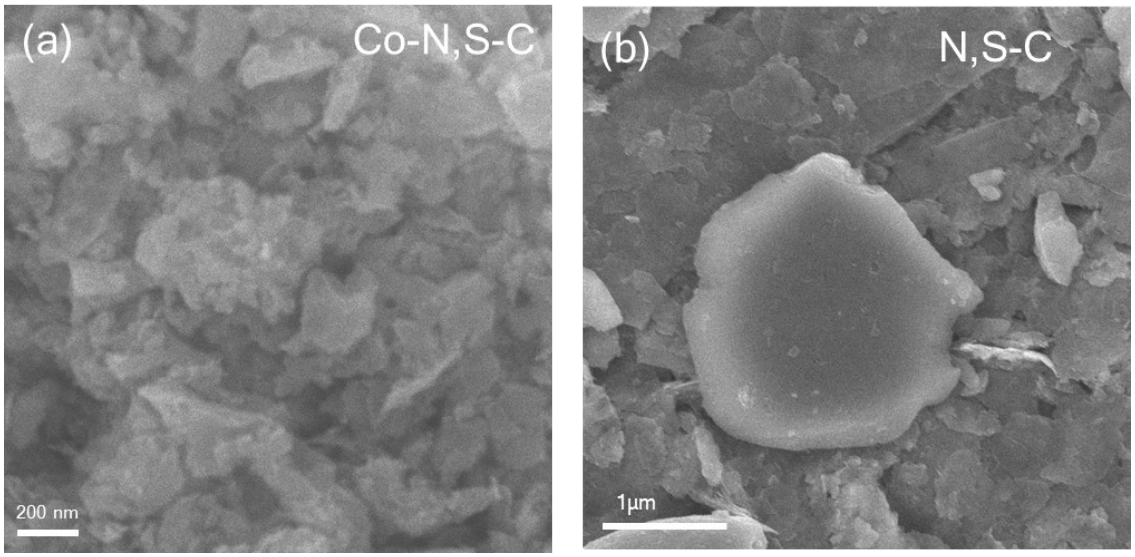

Fig. S3 (a) SEM images of (a) Co-N,S-C. (b) N,S-C.

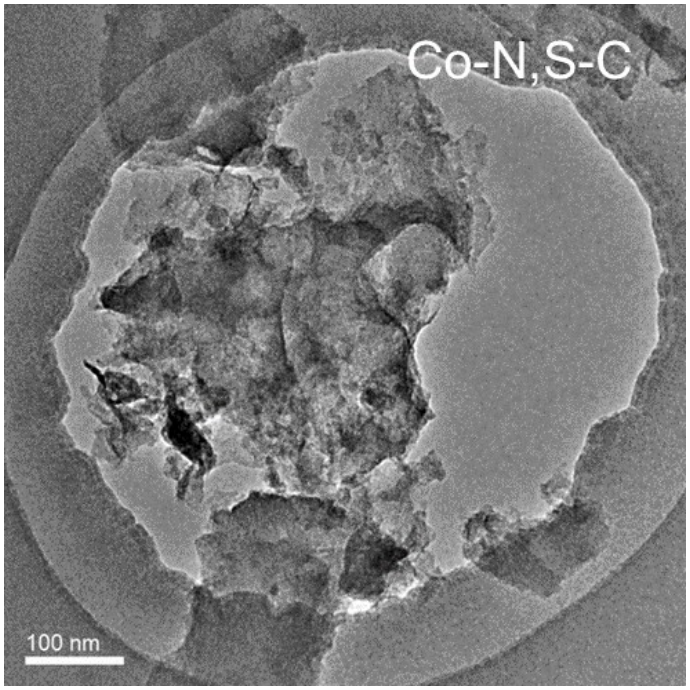

Fig. S4 TEM image of Co-N,S-C.

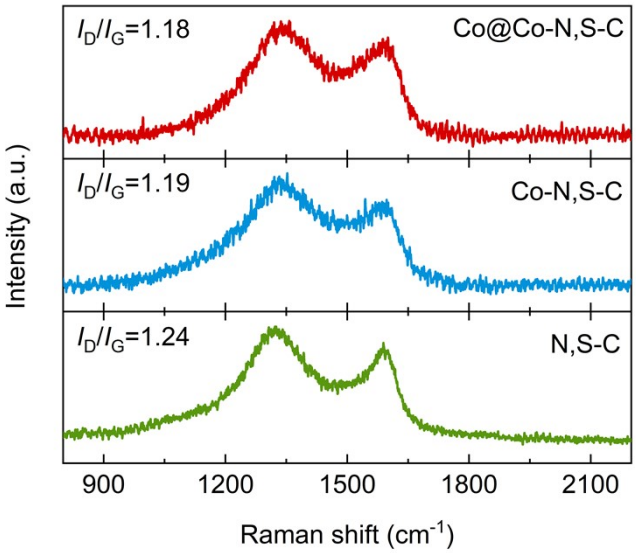

Fig. S5 Raman spectra of Co@Co-N,S-C, Co-N,S-C and N,S-C.

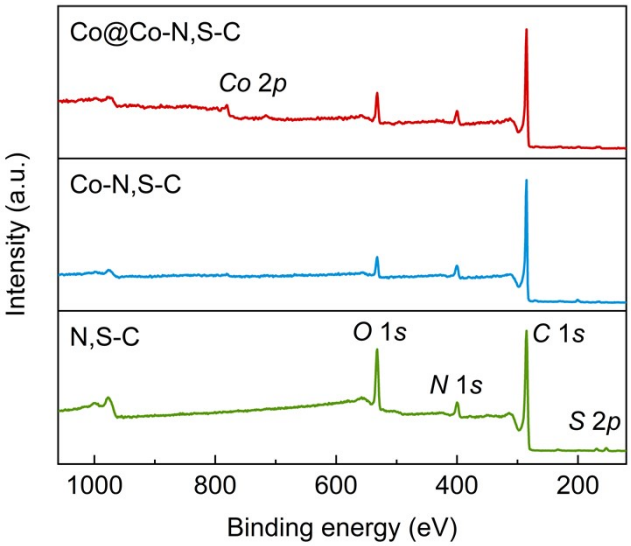

Fig. S6 XPS survey spectra of Co@Co-N,S-C, Co-N,S-C and N,S-C.

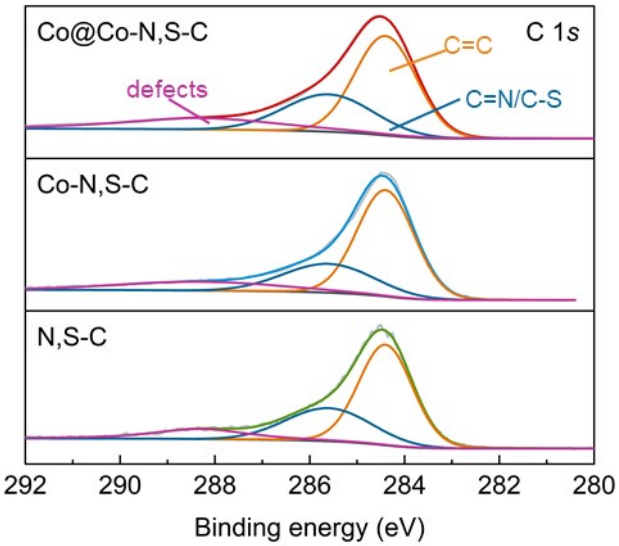

Fig. S7 The C 1*s* high-resolution XPS spectra of Co@Co-N,S-C, Co-N,S-C and N,S-C.

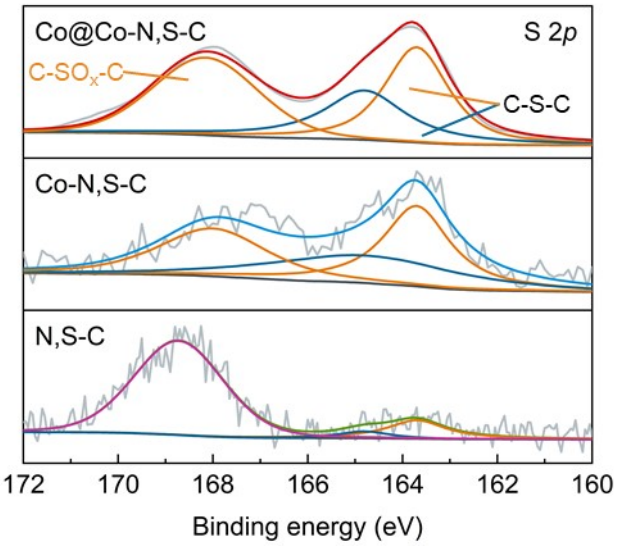

Fig. S8 The S 2*p* high-resolution XPS spectra of Co@Co-N,S-C, Co-N,S-C and N,S-C

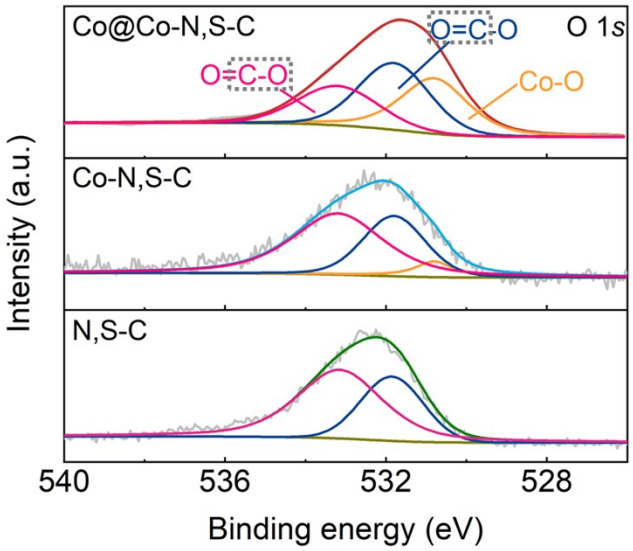

Fig. S9 The O 1*s* high-resolution XPS spectra of Co@Co-N,S-C, Co-N,S-C, and N,S-C.

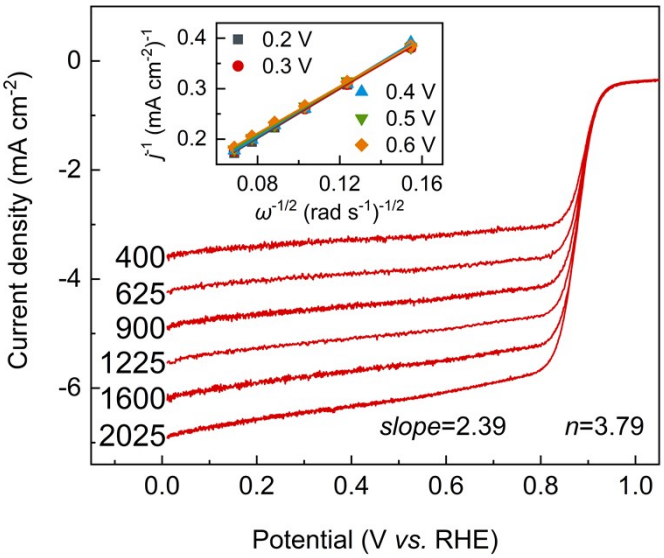

Fig. S10 LSV curves of Co@Co-N,S-C in O_2-saturated 0.1 M KOH at a sweep rate of 5 mV s^{-1} with the different rotation rates (400-2025 rpm). Inset: corresponding K-L plots at different potentials.

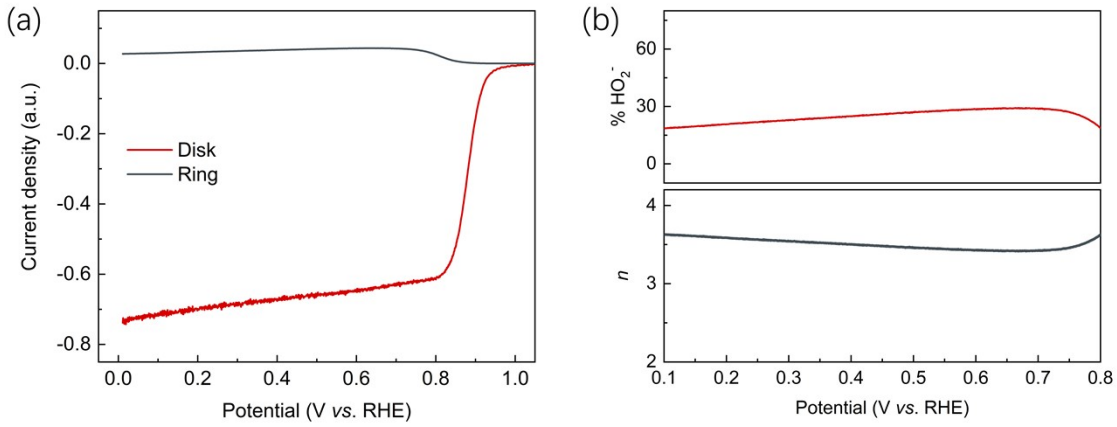

Fig. S11 RRDE voltammograms recorded with Co@Co-N,S-C in O_2-saturated 0.1 M KOH at 1600 rpm. The disk potential was scanned at 5 mV s^{-1}, and the ring potential was constant at 1.5 V. b) The calculated peroxide percentage (% HO_2^-, the upper half) and the electron transfer number (the lower half) at various potentials calculated from the corresponding RRDE data in a).

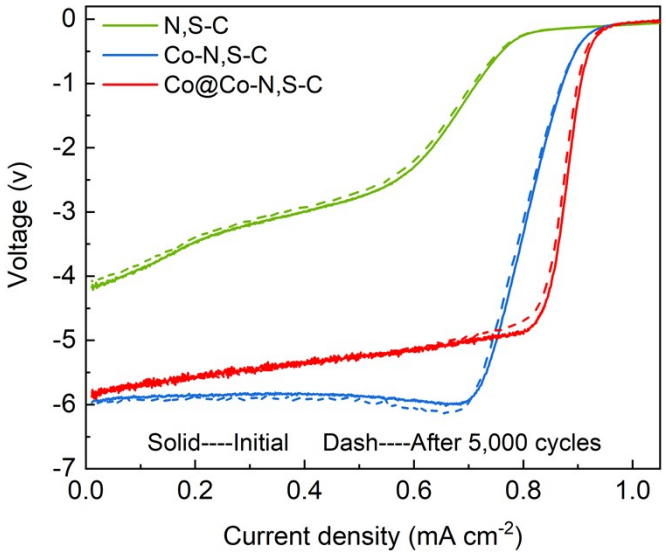

Fig. S12 The ORR LSV curves of Co@Co-N,S-C, Co-N,S-C, and N,S-C before and after 5000 potential cycles between 0.6 and 1.1 V.

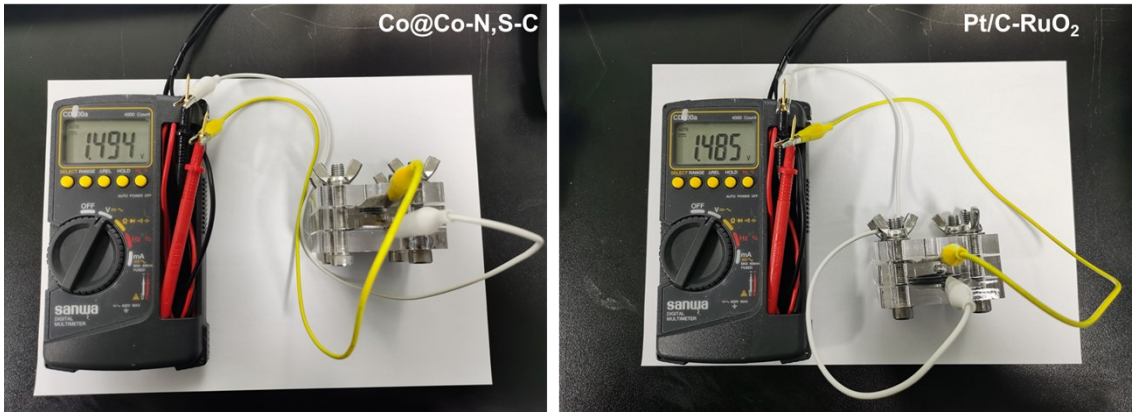

Fig. S13 Photos of the OCP of two aqueous zinc-air batteries based on Co@Co-N,S-C and Pt/C-RuO_2.

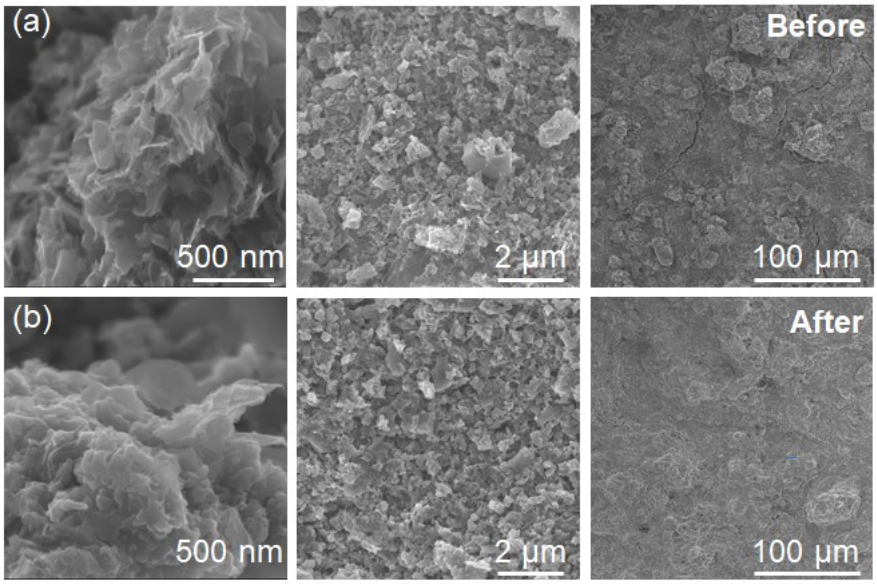

Fig. S14 SEM images of the air electrode with Co@Co-N,S-C as catalytic layers (a) before and (b) after long-term cycling.

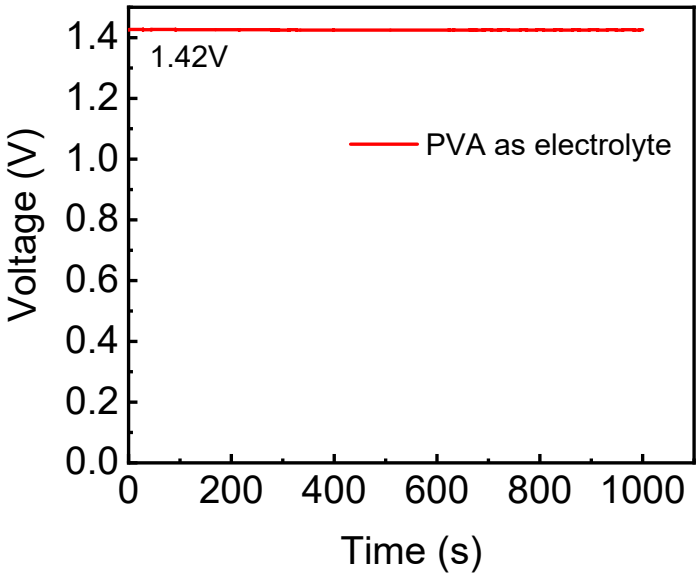

Fig. S15 The OCP of Co@Co-N,S-C-based solid-state rechargeable zinc-air battery.

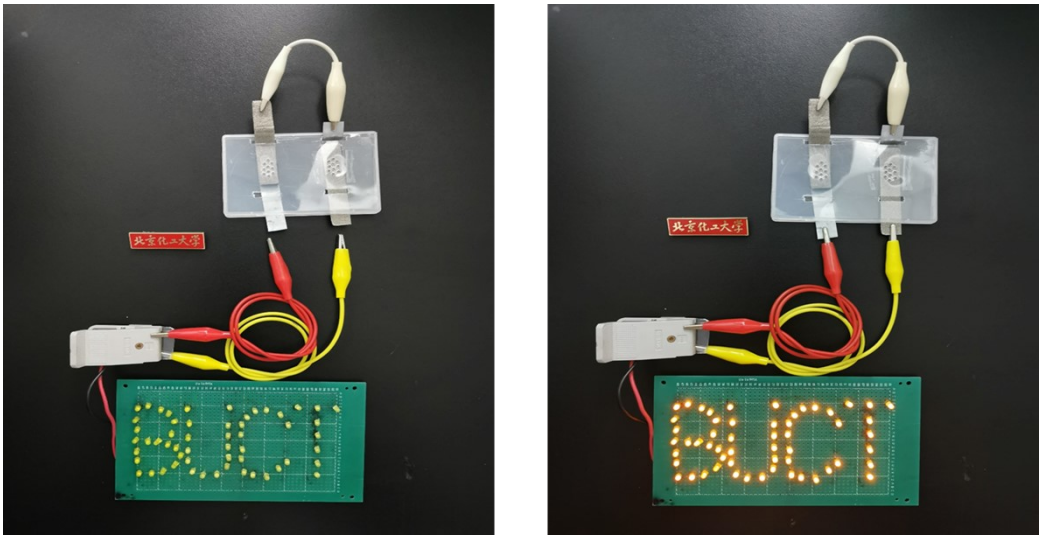

Fig. S16 Two tandem solid-state batteries could provide power for a series of LED lamps.

Table S1 The C-, N-, O-, S- and Co- content of Co@Co-N,S-C, Co-N,S-C and N,S-C measured by the corresponding XPS date.

Samples	C / (at.%)	N / (at.%)	S / (at.%)	Co / (at.%)	O / (at.%)
Co@Co-N,S-C	80.29	8.69	0.94	1.23	8.85
Co-N,S-C	84.5	6.4	0.63	0.35	8.11
N,S-C	75.77	7.02	0.86	----	16.36

Table S2 Summary of the bifunctional catalytic activities of the recently reported electrocatalysts.

Catalyst	$E_{1/2}$ / V	$E_{j=10}$ / V	ΔE / V	Electrolytes	Reference
Co@Co-N,S-C	0.88	1.62	0.74	0.1 M KOH	This work
Pt/C-RuO_2	0.84	1.60	0.76	0.1 M KOH	This work
CoDNG900	0.827	1.577	0.75	0.1 M KOH	*Appl Catal B-Environ* **2021,** *281*, 119514
NSC/Co_9S_8-200	0.83	1.63	0.8	0.1 M KOH	*Nano Energy* **2022,** *92*, 106750
FeNCFs	0.84	1.63	0.79	0.1 M KOH	*Carbon* **2022,** *187*, 196-206
CNT@SAC-Co/NCP	0.87	1.61	0.74	0.1 M KOH	*Adv. Funct. Mater.* **2021,** *31* (42), 2103360
Co/CNWs/CNFs	0.82	1.64	0.82	0.1 M KOH (ORR) 1 M KOH (OER)	*Adv. Funct. Mater.* **2021,** *31* (43), 2105021
FeCo/Co_2P@NPCF	0.79	1.56	0.77	0.1 M KOH	*Adv. Energy Mater.* **2020,** *10* (10), 1903854
FeNi@NCNT-CP	0.85	1.59	0.74	0.1 M KOH	*Small* **2021,** *17* (4), 2006183
FeCo/NSC	0.82	1.56	0.74	0.1 M KOH	*J. Energy Chem.* **2021,** *56*, 64-71

References

(1) Ravel B.; Newville M. *J. Synchrotron Radiat.* **2005**, *12*, 537-541.

(2) Knecht M. R.; Weir M. G.; Frenkel A. I.; Crooks R. M. *Chem. Mater.* **2008**, *20*, 1019-1028.

(3) Duce C.; Porta V. D.; Bramanti E.; Campanella B.; Spepi A.; Tine M. R. *Nanotechnology* **2017**, *28*, 055706.

(4) Huang Y.; Luo Y.; Zheng W.; Chen T. *ACS Appl. Mater. Interfaces* **2014**, *6*, 19217−19228.